Korean Journal of Chemical Engineering (2024) 41:2277–2285
https://doi.org/10.1007/s11814-024-00192-4

ORIGINAL ARTICLE

Systematic Narrowing of ZIF-8 Apertures via Controlled 2-Ethylimidazole Doping for Hydrogen/Carbon Dioxide Separation

Lee Yang[1] · Sunghwan Park[2] · Wong Zhong Han[1] · Musab Abdul Razak[1] · Lee Yong Zhen[1] · Muhammed Faires[1] · Rozita Omar[1] · Thomas Shean Yeaw Choong[1] · Rosiah Rohani[3] · Mohamad Rezi Abdul Hamid[1]

Received: 13 January 2024 / Revised: 4 May 2024 / Accepted: 6 May 2024 / Published online: 20 May 2024

Abstract

Sodalite (SOD) zeolitic-imidazolate frameworks (ZIFs) with uniform angstrom scale apertures can offer high gas sieving ability for separation applications. Fixed apertures of ZIFs can effectively separate specific gas pair but may not be able to provide similar level of separation for larger or smaller gas pairs. Multivariate (i.e., mixed-linker) ZIFs with controlled linker incorporation can provide desired aperture tuning but difficult to synthesize especially when incorporating linkers that would normally form different structures. Herein, we report a systematic narrowing of SOD ZIF-8 by partially replacing 2-methylimidazole (mIm) linkers of ZIF-8 with 2-ethylimidazole (eIm) via delayed linker addition (DLA) method. Percentages of eIm in the hybrid frameworks were determined to be around 14.3%, 9.1%, and 5.1% for ZIF-8 nuclei formed in 5, 12.5, and 20 min, respectively. Ethyl moiety of eIm restricts framework flexibility of the hybrid ZIF-8, shifts ZIF-8 gate-opening pressure to higher value, and eventually diminishes the gate-opening effect. Polysulfone (PSF)-based mixed-matrix membranes utilizing eIm-doped ZIF-8 as fillers displayed slight reduction in CO_2 permeability (18.56 Barrer to 14.85 Barrer) which result in H_2/CO_2 ideal selectivity improvement. DLA method is expected to work well for other imidazole-based linkers and can perhaps be used to synthesize mixed-linker of other SOD ZIFs.

Keywords Metal–organic frameworks · Zeolitic-imidazole frameworks · Hybrid ZIFs · Mixed-matrix membranes · Gas separations

Introduction

Hydrogen (H_2) is a key element in future energy transition from the traditional fossil fuel source. Membrane-based H_2 production is considered more energy efficient and require relatively low capital and operating expenditures [1]. Most of commercial membranes are made from synthetic polymers because they are inexpensive and easy to manufacture on large scale. Typical polymer membranes unfortunately have low H_2/CO_2 selectivity and/or CO_2 permeability owing to their trade-offs, limiting the separation performance below the upper-bound [2]. With respect to these, mixed-matrix membranes (MMMs) have long been considered to overcome the fundamental limitation of polymeric membranes. MMM fabrication involve blending of nanoparticles, particularly those with high gas sieving ability, such as metal–organic frameworks (MOFs) or zeolites into continuous polymer matrix to improve the membrane selectivity, permeability, or both [3, 4]. MMMs utilizing fillers with open frameworks and appropriately sized apertures can provide high H_2/CO_2 selectivity while maintaining similar/higher gas throughput. The composite membranes are expected to possess enhanced stability compared to traditional polymer membranes and more importantly the

Lee Yang and Sunghwan Park are contributed equally to this work.

✉ Mohamad Rezi Abdul Hamid
m_rezi@upm.edu.my

[1] Department of Chemical and Environmental Engineering, Universiti Putra Malaysia, 43400 Serdang, Selangor, Malaysia

[2] Department of Energy Chemical Engineering, Department of Advanced Science and Technology Convergence, and Convergence Research Center of Mechanical and Chemical Engineering (CRCMCE), Kyungpook National University, Sangju-Si 37224, Republic of Korea

[3] Department of Chemical and Process Engineering, Faculty of Engineering and Built Environment, Universiti Kebangsaan Malaysia, 43600 Bangi, Selangor, Malaysia

membrane transport properties are customizable to target a specific gas mixture.

Zeolitic-imidazole frameworks (ZIFs) [5, 6], a sub-class of MOFs, have been utilized for various applications due to their highly tunable physical/chemical properties, chemical/thermal stabilities as well as well-defined crystal structures. SOD ZIF-8 consisting of 2-methylimidazolate linkers tetrahedrally coordinated to divalent zinc ions has been intensively investigated for gas separations [7]. The relatively narrow six-membered ring aperture of 3.4 Å, defined crystallographically, makes ZIF-8 a potential molecular sieve material for H_2/CO_2 separation. Utilizing ZIF-8 as filler for MMM fabrication would help boost the membrane performances beyond the polymer upper-bound. The linker flip-flopping motions of ZIF-8, however, extend the pore size, allowing the penetration of much larger gas molecules than 3.4 Å [8]. The extent of the effective pore sizes varies in response to different types of guest molecules [9]. Despite showing excellent C_3H_6/C_3H_8 separation performance (C_3H_6/C_3H_8 selectivity > 100 can be achieved), ZIF-8 fails to offer similar performance level for H_2/CO_2 mixture with most of the fabricated membranes showing selectivity of < 10 [7].

One of the fundamental limitations of ZIFs being a crystalline material is its fixed apertures. Fixed apertures of ZIFs can provide high resolution separation of a specific gas mixture, but it may not be able to provide a similar level of separation for other gas mixture, in this case H_2/CO_2. That said, for effective CO_2 separations, a strategy to narrow the aperture and restrict framework flexibility of ZIF-8 while maintaining its topology is highly demanded. Mixing various bridging ligands or metal centers of MOFs/ZIFs (often referred as hybrid strategy) can alter the materials' physical or chemical characters (e.g., porosities, pore sizes, polarity, etc.) as demonstrated in a number of works [10–12]. ZIF-7 (benzimidazole linker), ZIF-8 (2-methylimidazole linker), ZIF-90 (2-imidazolecarboxaldehyde linker), ZIF-67 (cobalt metal center), and CdIF-1 (cadmium metal center) are examples of MOFs/ZIFs with similar SOD structure (iso-structure). So, one can expect that hybrid of these ZIFs would possess a similar topology. In fact, a variety of multivariate (mixed-metal or mixed-linker) ZIFs maintaining its SOD network such Co-Zn-ZIF-8 [12, 13], Cd-Zn-ZIF-8 [14], ZIF-7-8 [15, 16], and ZIF-8-90 [10, 17] with secondary linker/metal proportions from 0 to 100% have been successfully synthesized. Meanwhile, mixing non-isostructural ZIFs linkers such as 2-ethylimidazole (ZIF-14 ANA) and imidazole (e.g., ZIF-3 DFT, ZIF-4 CAG, ZIF-10 MER, etc.) with mIm linker of SOD ZIF-8 might not produce the desired topology and in most cases can only allow a small percentage of incorporation [5].

There are a few notable works attempting to incorporate non-isostructural eIm linker into SOD ZIF-8. The dramatic restriction of the linker motion of ZIF-8 by introducing eIm linkers was first observed by Hillman et al. [18]. A high magnetic field pulsed field gradient (PFG) nuclear magnetic resonance (NMR) was utilized to study the self-diffusion of gasses in eIm-modified ZIF-8 with linker content up to 22.2 mol% [19]. It was found that the eIm linker substitution resulted in an increase the intracrystalline diffusivities of the C_2H_4, C_2H_6, and C_3H_6 despite the restricted linker motion. Park et al. [20] attempted to improve the separation performance of MMMs containing ZIF-8 by adding eIm linkers. The resulting membranes similarly showed an increase in C_3H_6 permeance at relatively low eIm loadings with negligible change in the separation factor. Higher eIm incorporation between 40 and 60 mol% eventually enhance C_3H_6/C_3H_8 separation factor toward commercially attractive region [20]. In light of these, by controlling the amount of eIm used, it is possible to tune the aperture size of the ZIF-8 and optimize H_2/CO_2 separations performance of eIm-doped ZIF-8 MMMs.

It is worth to mention that incorporating non-isostructural eIm linker in ZIF-8 SOD frameworks via a direct mixing approach sometimes does not produce the desired hybrids as observed by Huang et al. [21]. In an attempt to mix eIm and mIm together to form a hybrid ZIFs, they ended up with a physical mixture of ZIF-8 ($Zn[mIm]_2$) with SOD topology and ZIF-14 ($Zn[mIm]_2$) with ANA topology. Recently, Jeong's group reported a novel method, which they refer to "delayed-linker addition" (DLA) method to enlarge ZIF-8 framework by incorporating another non-isostructural linker (i.e., imidazole, Im) without forming new crystal phase or altering the original crystal structure [22]. The percentage of Im incorporation as high as ~ 65% was reported which is unprecedented. Given this success, we hypothesize the DLA method might be effective to incorporate eIm into ZIF-8. In this contribution, we demonstrate a controlled tuning of ZIF-8 aperture targeting H_2/CO_2 gas mixture. DLA approach takes advantage of partially grown ZIF-8 nuclei that require low nucleation energy penalty as a foundation to form dual-linker complexes. Narrowing of the ZIF-8 aperture can be achieved by incorporating bulky eIm linker in the framework and the extent of incorporation can be controlled by varying important synthesis parameter including nucleation time and eIm concentration.

In this work, we prepared eIm-incorporated ZIF hybrids using DLA method. A series of characterization tools were utilized to evaluate percentage of incorporation, structure, and microstructure of these ZIF hybrids. To demonstrate its feasibility for H_2/CO_2 separation, the prepared ZIFs were assessed by blending the crystals with PSF forming MMMs. Considering that estimation of transport properties of these hybrid ZIFs for H_2 and CO_2 has never been conducted before, the gas-separation data of this study can

serve as a basis to estimate transport behavior of other non-condensable gasses.

Materials and Methods

Materials

2-Methylimidazole ($C_4H_6N_2$, 99%, Sigma-Aldrich), 2-ethylimidazole ($C_5H_8N_2$, 99%, Thermo Scientific), zinc nitrate hexahydrate ($Zn(NO_3)_2.6H_2O$, 98%, reagent grade, Sigma-Aldrich), methanol (CH_3OH, analytical reagent grade, R&M Chemicals) were used as linker source, metal source, and solvent for the preparation of ZIF-8 and eIm-doped ZIF-8. Polysulfone (PSF, $MW_{avg} = 35{,}000$ g.mol^{-1}, Sigma Aldrich), and *N*,*N*-Dimethylformamide (DMF, 99.8%, extra dry, Thermo Scientific) were used to prepare neat PSF membranes and MMMs.

Synthesis of ZIF-8 and eIm-ZIF-8 Crystals

eIm-ZIF-8(*x*) (where *x* represent ZIF-8 nucleation time in min) were synthesized using DLA method previously developed by our group with a slight modification [22]. In brief, three separate methanolic solutions of ZnN, mIm, and eIm with molar concentration of 0.134 M, 1.067 M, and 4.831 M, respectively were prepared. After that, 15 ml of ZnN solution was added into 15 ml of mIm solution and the mixture was stirred at room temperature inside a beaker for 5 min (nucleation time). Next, 5 ml of eIm solution was added into the solution and stirred for 1 min. The mixture was immediately transferred into a microwave synthesizer and microwaved at a power of 80 W for 1.83 min (110 s). The microwave-assisted synthesis of hybrid ZIFs was performed in a single-phase stainless steel modified microwave oven (Panasonic, NN-ST340M, Panasonic, Japan) with a 206 mm (H) × 315 mm (W) × 353 mm (D) microwave oven cavity. The microwave was equipped with a 2.45 GHz magnetron and can operate at a maximum power output of 800 W. The mixture was then taken out from the microwave synthesizer and left to cool to room temperature for 30 min. The mixture was then centrifuged at 6000 RPM for 15 min and decanted to collect ZIF powders. To remove unreacted metals and linkers, the prepared crystals were washed with fresh methanol three times. Finally, the crystals were dried inside an oven at 65 °C overnight before use. Three eIm-ZIF-8(*x*) samples were prepared by varying nucleation time (5 min, 12.5 min, and 20 min). Pure ZIF-8 with nucleation time of 12.5 min (i.e., ZIF-8(12.5)) was also synthesized as a control. For ZIF-8(12.5), the solution was immediately microwaved after 12.5 min of nucleation time.

Synthesis of ZIF-8 and eIm-ZIF-8 Mixed-Matrix Membranes

10 wt% eIm-ZIF-8(x) asymmetric MMMs were prepared by blending respective ZIF crystals with PSF. First, PSF pallets and ZIF powders were first dried inside an oven at 65 °C overnight to remove residual solvent and moisture. The fillers were then dispersed in DMF solvent and then sonicated in a bath sonicator (Elmasonic S30H) for 10 min with a 5 min rest time. This process was repeated for three times. Solvent-to-solid (i.e., polymer and filler) weight ratio used for the preparation of the membrane was 80:20. After that, PSF pallets were added into ZIF/solvent suspension and stirred vigorously at 60 °C for 24 h. ZIF/PSF dope solution was degassed at room temperature to remove air bubbles. ZIF/PSF dope solution was then poured on a glass substrate and casted using a manual film applicator with a clearance of 300 µm. The as-casted membranes are then immediately transferred into an oven preheated to 160 °C and the membranes were dried for 24 h. Neat PSF membrane was prepared following a similar procedure but without ZIF dispersion steps.

H_2 and CO_2 Single Gas Permeation Measurements

Single gas (i.e., H_2 and CO_2) permeation measurements for pure PSF membranes and ZIF-based MMMs were performed at room temperature under at a pressure of 4.3 bar using a dead-end setup. A membrane with an active membrane area of 2.29×10^{-3} m^2 (diameter 5.4×10^{-2} m) was loaded into a custom-made permeation cell (Fig. S1) and secured to the gas permeation setup. Pure H_2 or CO_2 gasses at pressure of 4.3 bar was supplied to the feed side. Volumetric flow rates at the permeate side was measured using a bubble flow meter.

Characterization

Fourier transform infrared (FTIR) spectra of the ZIF crystals were collected using a Perkin Elmer FTIR Spectrometer Frontier scanning within a wavenumber range of 400–4000 cm^{-1} (scan resolution of 1 cm^{-1} and 16 number of scan). Crystallinities and phases of ZIF-8 and eIm-ZIF-8(*x*) crystals were determined by X-Ray diffraction (XRD) on Rigaku Dmax/rA diffractometer (Cu-Kα radiation = 1.542 Å) with a 2θ scan range of 5° – 40° and scan step size of 0.02°. Surface area and nitrogen adsorption–desorption isotherm measurements were carried out on a Micromeritics 3Flex Adsorption Analyzer at 77 K. Prior to adsorption measurements, the samples were activated at 150 °C for 9 h. Secondary linker (i.e., eIm) compositions in the parent ZIF-8 frameworks were determined using solution proton nuclear magnetic resonance (^{1}H-NMR, Bruker

Avance III HD 400 MHz). Solution NMR samples were prepared by digesting ZIF samples in deuterated acetic acid-d4. Morphologies of the powders and membranes were observed using scanning electron microscope (SEM) Hitachi S3400N operating at acceleration voltage of 15 kV. Membrane samples were freeze fractured in liquid nitrogen to obtain clean cross section. All samples were sputter coated with conductive materials prior to imaging.

Results and Discussion

Synthesis of ZIF-8 and eIm-Doped ZIF-8

Hybrid ZIF-8 of various secondary eIm linker incorporation were prepared using DLA method previously reported [22]. Combining two non-isostructural ZIFs (e.g., $Zn(eIm)_2$ with ANA network with $Zn(mIm)_2$ with SOD network) is non-trivial as both possess different crystal system. In most cases, only a small fraction of non-isostructural secondary linker can be incorporated into the parent frameworks without disrupting the material crystal structure. DLA method enables a high incorporation of non-isostructural linkers such as 2-ethylimidazole, imidazole, and 2-phenylimidazole into ZIF-8 without altering its SOD topology. In DLA approach, mixing of secondary linkers is purposely delayed after stable ZIF-8 nuclei are formed. DLA method begins with formation of ZIF-8 clusters as shown in Fig. 1. Three ZIF-8 nucleation times of 5 min, 12.5 min, and 20 min are selected to represent different crystallization phases of ZIF-8 [23]. It is worth to mention that nucleation time of less than 5 min is insufficient to create stable ZIF-8 nuclei, hence ignored in this work. Secondary eIm linkers are introduced into the ZIF-8 colloidal solution before the nuclei developed into well-defined crystals. The mixture is subjected to a microwave heating to form mIm-eIm dual linker ZIF-8 (i.e., eIm-ZIF-8(x) where x represents ZIF nucleation time in min).

Electron micrographs of eIm-ZIF-8(x) prepared under different nucleation time are presented in Fig. 2. It is worth noting that the prepared hybrid crystals, including ZIF-8 prepared under microwaves have a similar white appearance as shown in the inset images. Morphologies of individual crystal grains for eIm-ZIF-8(x) are identical with all having sharp hexagonal facets and size of ~ 230 nm, similar to that of pure ZIF-8 crystals prepared under nucleation time of 12.5 min (i.e., ZIF-8(12.5)). Note that, ZIF-8(12.5) samples are immediately microwaved under a similar condition without secondary linker addition steps.

Structure Evaluation of eIm-Doped ZIF-8

Figure 3 showed powder X-Ray diffraction patterns (XRD) of ZIF-8 and eIm-doped ZIF-8 with various secondary linker incorporation. Pure ZIF-8 (i.e., ZIF-8(12.5)) XRD pattern displayed characteristic peak positions well-matched with theoretical pattern of SOD ZIF-8 which agrees to those previously reported [24]. ZIF-8 signature peaks at 2θ of 7.4°, 10.5°, 12.8°, and 14.8° can be indexed to the 110, 200, 211, and 220 crystallographic planes of ZIF-8, respectively. Despite a slight shift in diffraction peaks for ZIF samples compared to the simulated one, which is likely due to systematic error of the XRD instrument, there are no apparent shifts in d-spacing upon introducing the secondary linker (eIm) in ZIF-8. Well-defined peaks of various eIm-doped ZIF-8 corresponding to that of pure and simulated ZIF-8 confirms hybrid ZIFs with high degree of crystallinities that maintains a similar cubic unit cell of I-43 m space group of ZIF-8 [12]. It is worth noting that DLA strategy allows for high incorporation of non-isostructural eIm linker without disrupting or creating new network structure unlike the conventional mixing strategy reported by Huang et al. [21]. In their work, they attempted to synthesize a hybrid ZIF by directly adding eIm/mIm mixture into metal (i.e., Zn) solution. A single-phase mixed-ligand complexes was expected to form given the similar coordination ability of both linkers. As opposed to obtaining a single-phase SOD eIm-ZIF-8, the precipitate collected however was found to just be a physical mixture of two different ZIFs with ZIF-8 ($Zn(mIm)_2$, SOD

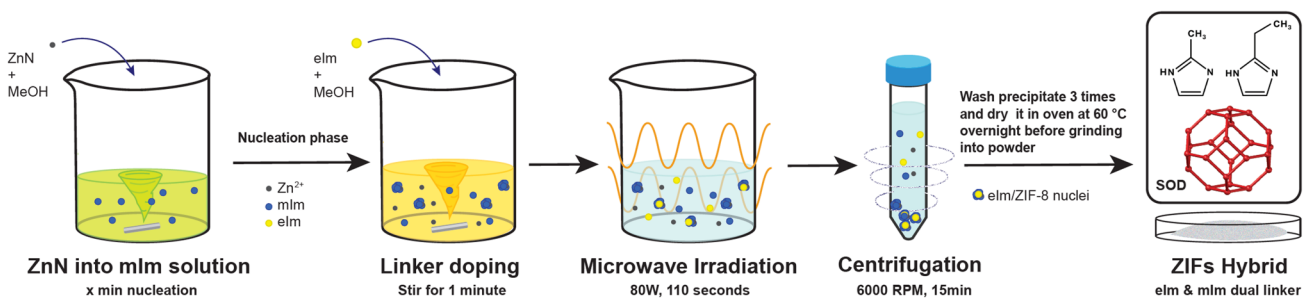

Fig. 1 Schematic illustration of microwave-based synthesis of ZIF-8 and eIm-ZIF-8(x) using DLA method

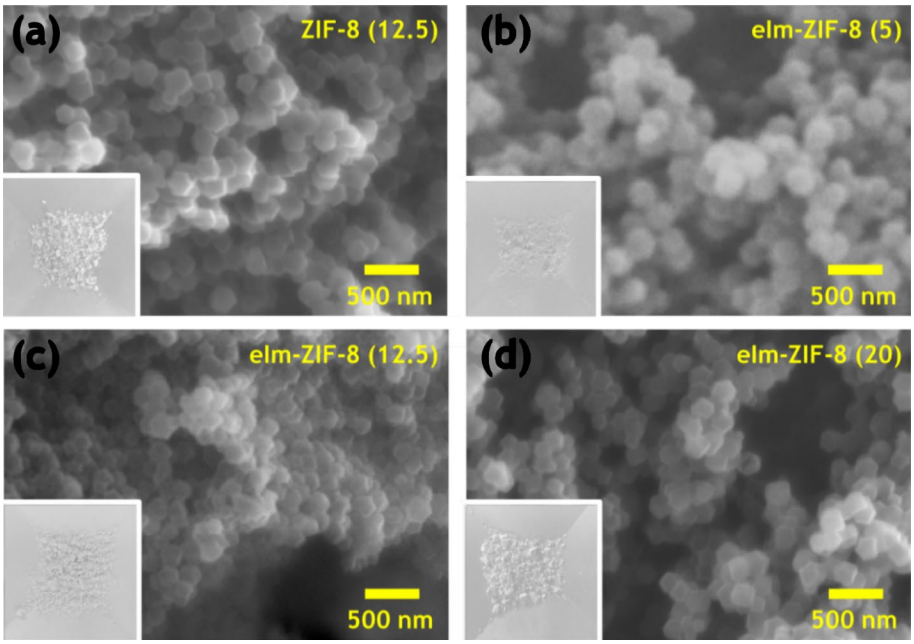

Fig. 2 Electron micrographs of ZIF-8 and eIm-ZIF-8(*x*) crystals. Inset images show a digital photographs of the prepared-ZIF powders

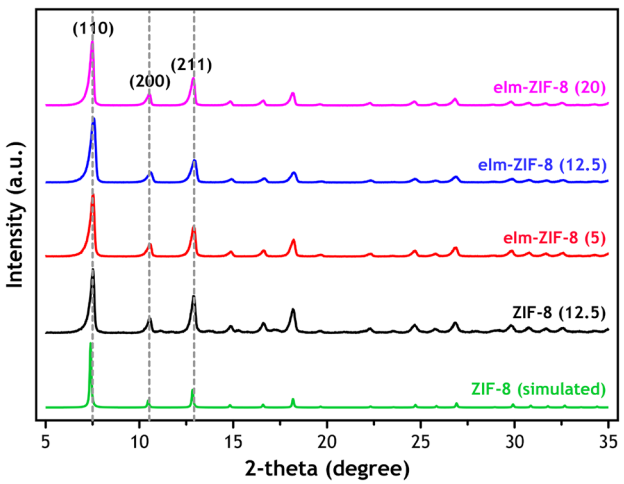

Fig. 3 Powder X-Ray diffraction pattern of ZIF-8 and eIm-ZIF-8(*x*)

topology) as major product and ZIF-14 ($Zn(eIm)_2$, ANA topology) as minor product.

FTIR spectra of eIm-doped ZIF-8 with various linker percentages are compared with pure ZIF-8 (Fig. 4). All ZIF samples displayed identical signature IR bands at 421 cm^{-1} and 1,145 cm^{-1} which can be ascribed to Zn–N and C–N bonds of ZIF-8 [25]. Despite the red shift of the major Zn–N vibration peak at 421 cm^{-1}, the broadening of peaks in the range of 445–400 cm^{-1} toward higher wavenumbers suggests potential blue shifts for some components (Fig. 4). The emergence and increasing intensity of a peak at 443 cm^{-1} in eIm-ZIF-8(x) with increasing eIm contents in Fig. S2, suggest the presence of higher frequency vibrations. It was hypothesized that due to the heterogeneous distribution of eIm by DLA, which contrasts with previous eIm-ZIFs synthesized by de novo methods [18, 20], the Zn–N bond

Fig. 4 FTIR spectra of ZIF-8 and eIm-ZIF-8(*x*)

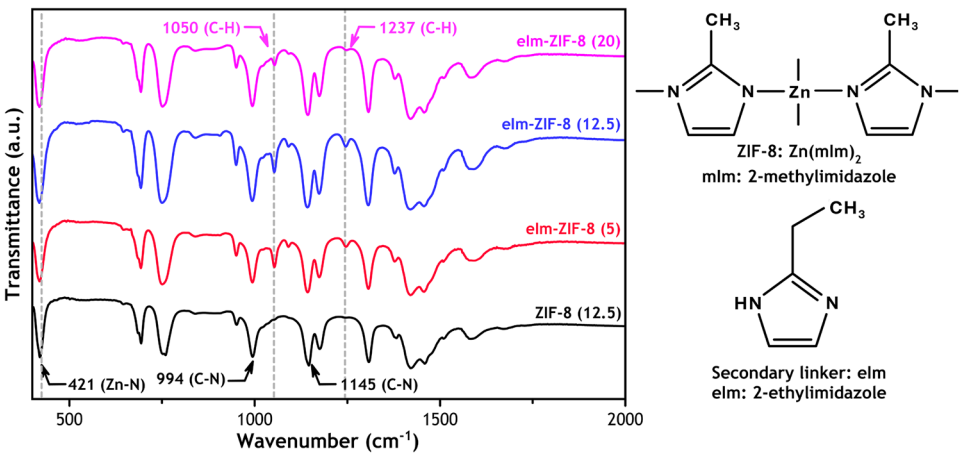

stiffening indicated by the blue shift occurs locally. The locally restricted flip-flopping motion of the ZIF frameworks likely reduce the effective aperture size of the eIm-doped ZIF-8. Two new bands at 1050 $cm^{-1}$and 1237 cm^{-1} appears for the eIm-doped ZIF-8 belonging to the $–CH_3$ out-of-plane rocking and C–H in plane bending modes of eIm linkers, respectively [18, 26]. The appearance of the new bands observed under infrared therefore indicates that secondary eIm linkers have been successfully incorporated into ZIF-8 frameworks.

^{1}H-NMR analysis was performed to determine the actual compositions of eIm dopant in the parent ZIF-8 frameworks. For eIm linkers, NMR spectra displayed two signals of $–CH_2$ quadruplet proton at ~ 3.1 ppm and $–CH_3$ triplet proton at ~ 1.4 ppm as depicted in Fig. 5 (see also Fig. S3). Based on the ^{1}H-NMR analysis, the percentages of secondary eIm linkers in parent ZIF-8 frameworks were estimated 14.3%, 9.1%, and 5.1% for eIm-doped ZIF-8 synthesized at 5 min, 12.5 min, and 20 min nucleation time, respectively, consistent with previous observations [22]. A foundation of DLA method is utilizing a half-formed, but stable ZIF-8 nuclei as a framework foundation to aid incorporation of secondary linker into the SOD network of ZIF-8. Allowing longer nucleation time produces larger and a more defined ZIF-8 crystals with characteristics resembling that of fully grown ZIF-8 which prevent further eIm incorporation, hence lower eIm fraction in the hybrid ZIFs. Computational studies by Jeong's group revealed that the energy penalty of incorporating secondary linker increases with nuclei sizes which further explain a decrease in eIm incorporation with longer nucleation time [22]. In addition to crystal nucleation time, we also investigated the effect of eIm starting concentration. Under a similar nucleation time of 5 min, increasing original eIm concentration by 1.5 × increases eIm percentage incorporation from 14.3 to 20.7% (see Fig. S4). It is worth to note that highest eIm percentage incorporation obtained in this work is lower than those reported by Hillman et al. [22] (14.5% vs 31.0%) likely due to lower eIm starting concentration (4.83 M vs 9.66 M) and microwave power input (80 W vs 100 W).

Nitrogen Physisorption Properties of eIm-Doped ZIF-8

Figure 6 presents N_2 physisorption measurements of ZIF-8 and eIm-ZIF-8(x). All samples displayed a Type I adsorption isotherm characteristic of ordered microporous materials (see Fig. S5). Several observations can be made when plotting the isotherm profiles in log scale. As shown in Fig. 6, there were two threshold pressure of sudden rise in N_2 uptakes occurring at relative pressure (P/P_o) of ~ 1.0×10^{-4} and 2.0×10^{-2} which are referred as "gate-opening" [27]. There are negligible shifts of the second gate-opening pressure, while the extent of pore volume changes by the second gate-opening is gradually diminished with higher eIm incorporation which is consistent with those previously reported [18, 20]. We postulate that bulky ethyl moiety of eIm linker add constriction in the hybrid framework, making it less flexible, thereby suppressing the structure change at a certain pressure. Diminishing of the "gate-opening" of ZIF-8 has been previously observed as well when the mIm linker of ZIF-8 is replaced with bulky benzimidazole linkers [10].

Surface areas and pore characters of the hybrid ZIFs are tabulated in Table 1. The estimated Brunauer-Emmet-Teller (BET) surface area of pristine ZIF-8 is 1701 $m^2.g^{-1}$, consistent with those previously reported [5, 20]. The BET surface areas for the hybrid ZIFs were lower than that of pristine ZIF-8. Interestingly, the surface areas systematically decrease with higher eIm incorporation in the following order: eIm-ZIF-8(20) – 1679 $m^2.g^{-1}$ > eIm-ZIF-8(12.5) – 1577 $m^2.g^{-1}$ > eIm-ZIF-8(5) – 1537 $m^2.g^{-1}$. Similarly, pore

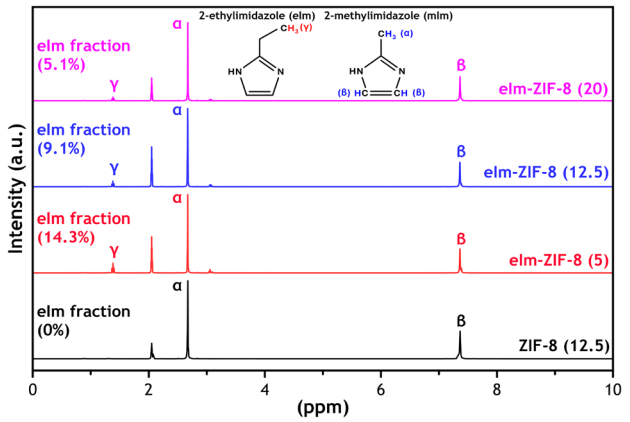

Fig. 5 ^{1}H-NMR spectra of ZIF-8 and eIm-ZIF-8(x) crystals

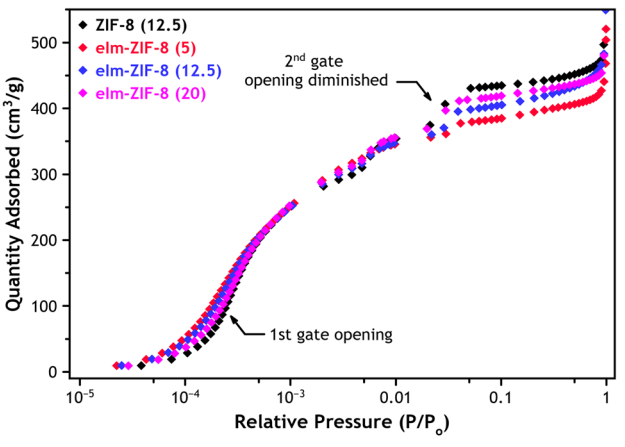

Fig. 6 N_2 adsorption isotherm (log scale) of ZIF-8 and eIm-ZIF-8(x) crystals

Table 1 Surface area and pore volume of ZIF-8 and eIm-ZIF-8(x) crystals

Sample	Surface area (m^2/g)		Pore volume* (cm^3/g)	Pore width* (Å)
	Langmuir	BET		
ZIF-8(12.5)	1918	1701	0.63	8.41
eIm-ZIF-8(20)	1856	1679	0.59	8.32
eIm-ZIF-8(12.5)	1796	1577	0.55	8.23
eIm-ZIF-8(5)	1714	1537	0.52	8.12

*Horvath–Kawazoe pore volume and median pore width

width and pore volume of the hybrid ZIFs calculated using Horvath–Kawazoe method decreases as well with higher eIm percentages in the frameworks. Narrowing of pore volume and pore width of the hybrid observed for the hybrid ZIF is likely due to incorporation of bulky eIm linkers in the frameworks.

eIm-ZIF-8(x) Mixed-Matrix Membranes (MMMs) for H_2/CO_2 Separation

We hypothesized pore narrowing of the six-membered ring apertures of the eIm-doped ZIF-8 would reduce transport diffusivity of CO_2 more so than that of H_2, consequently improves H_2/CO_2 diffusion selectivity [15]. It is important to point out that determination of transport properties of eIm-doped ZIF-8 for non-condensable gasses such as H_2 and CO_2 have not been determined either experimentally or computationally. To test this, we fabricated ZIF-8 and eIm-doped ZIF-8 dense MMMs with a similar filler loading of 10 wt% and later compare the membranes' H_2/CO_2 separation performances. Low filler loading is selected to minimize potential agglomeration or any polymer-filler interfacial defects. PSF is selected as polymer matrix due to its economic scalability, a good compatibility with ZIF-8, and potential for separating H_2 from H_2/CO_2 mixtures [2, 28]. MMMs with 10 wt% filler loading were prepared by physically blending respective eIm-ZIF-8(x) with PSF followed by solvent evaporation step. For neat PSF membranes, a similar procedure was conducted without blending with ZIF fillers. Performances of MMMs with eIm-ZIF-8(20) fillers were not investigated as the eIm content was below the percolation threshold (5.1%), which refers to the critical concentration of the dopant, eIm linkers, within the eIm-ZIF-8 framework needed to induce a notable change in the pore properties [29]. Figure 7 cross-sectional electron micrographs of neat PSF membranes and ZIF-containing MMMs (see Fig. S6 for top SEM images of the membrane). Thicknesses of the membrane dense layer were comparable, which averaged 26.3 ± 2.1 µm. Neat PSF membrane has a smooth and defect-free surface. No obvious interfacial voids formed between PSF and ZIFs and no particle agglomerations were observed on the surface of the fractured MMMs.

H_2/CO_2 gas-separation performances of the as-prepared membranes were tested using dead-end setup at 4.3 bar pressure. As shown in Fig. 8, neat PSF membrane displayed H_2 and CO_2 permeability of 8.12 ± 0.94 Barrer and 4.82 ± 0.21 Barrer, respectively, agreeing with those

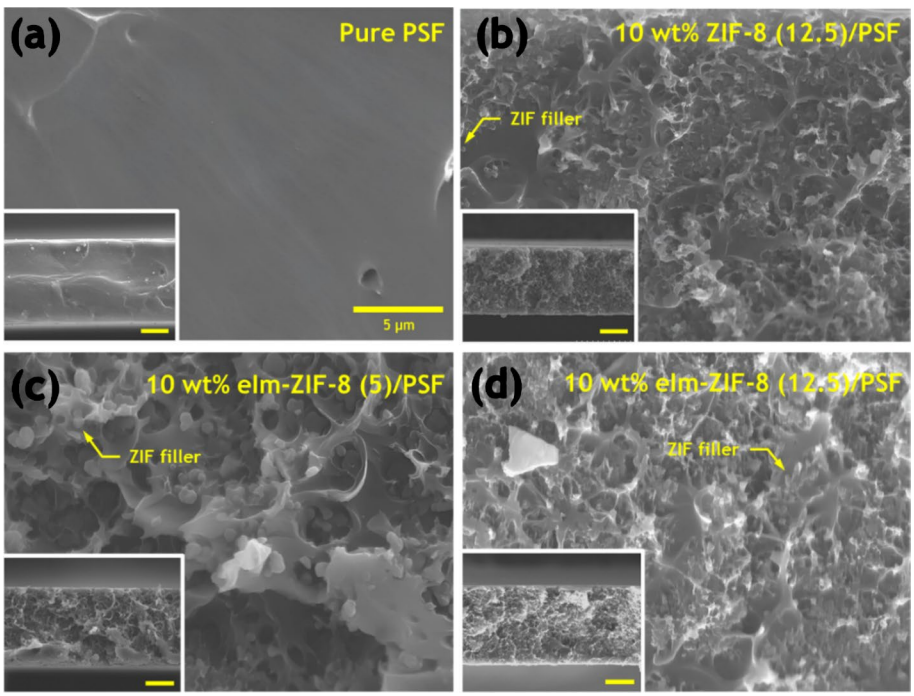

Fig. 7 Cross-sectional electron micrographs of the membranes: **a** pure PSF, **b** 10 wt% ZIF-8/PSF, **c** 10 wt% eIm-ZIF-8(5)/PSF and **d** 10 wt% eIm-ZIF-8(12.5). Scale of inset images correspond to 10 µm

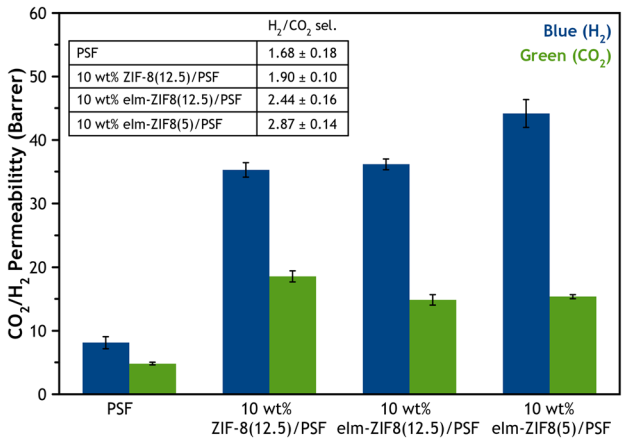

Fig. 8 H_2 and CO_2 pure gas-separation performance of membranes at 4.3 bar. Note. 1 Barrer = 3.348×10^{-16} mol.m.m^{-2}.s^{-1}.Pa^{-1}

previously reported [28, 30], supporting that the fabricated membranes are defect-free. A significant increase in both H_2 and CO_2 permeability was observed with the addition of ZIF-8 crystals when compared to those of neat PSF membranes (i.e., 35.29 ± 1.15 Barrer for H_2 and 18.56 ± 0.88 Barrer for CO_2), which also comes with a slight increase in H_2/CO_2 selectivity. The observed enhancements in gas permeance were likely due to the incorporation of highly porous crystalline ZIF-8, which increase gas diffusivity [31, 32]. Meanwhile, MMMs incorporated with eIm-ZIF-8(12.5) and eIm-ZIF-8(5) resulted in a reduction in CO_2 permeability to 14.85 ± 0.82 Barrer and 15.37 ± 0.33 Barrer, respectively. This decreasing trend in gas permeability with higher eIm fraction was also observed by Park et al. [20]. It was initially hypothesized that the restricted linker motion and narrower aperture of eIm-ZIF-8 lead to a significant decrease in CO_2 permeability, while H_2 permeability would remain unaffected or slightly decrease. In addition to diffusion factor, it should be noted that changes gas transport properties (i.e., permeability and selectivity) of the fabricated MMMs is also governed by adsorption factor. For eIm-ZIF-8 MMM, the unexpected increase in H_2 permeability was observed and this can be attributed to higher H_2 adsorption in eIm-ZIF-8 than that of in ZIF-8. Experimental and computational investigation such as H_2 and CO_2-adsorption isotherm / kinetics and molecular simulation of ZIF-8 and eIm-ZIF-8 are required to gain insight into this phenomenon.

Conclusions

Multivariate SOD ZIFs (e.g., mixed-linker) composed of several distinct functional units can provide the desired property tuning for separation applications. However, incorporating secondary ligands that would normally form different structures into SOD structures of ZIF-8 through a direct synthesis is challenging. In this work, aperture tuning (i.e., narrowing) of ZIF-8 was successfully performed using a robust DLA method, achieved without disrupting the SOD network of ZIF-8. Simple manipulation of ZIF-8 nucleation time enables a controlled tuning of eIm content in ZIF-8 frameworks. Dual linker ZIFs with different eIm percentage incorporations can be synthesized by simply delaying eIm linker addition in the synthesis solution. Hybrid ZIF-8 with 5.1%, 9.1%, and 14.3% eIm incorporation can be synthesized by delaying eIm addition by 20 min, 12.5 min, and 5 min, respectively. The presence of bulky ethyl moieties creates constriction in ZIF-8 structure, making it less flexible, consequently shifting the ZIF-8 gate-opening pressure. MMMs utilizing eIm-ZIF-8 displayed showed a slight reduction in CO_2 permeability than those MMMs with ZIF-8 filler (20.0% and 17.2% decrease in CO_2 permeability for MMMs containing 10% ZIF-8(12.5) and eIm-ZIF-8(5), respectively), attributable to narrower pore size which prevent fast transport of CO_2. To sum up, specific pore characters can be imparted to SOD ZIF-8 using DLA method. Given its utility and robustness, DLA method is expected to work well for other imidazole-based linkers and can perhaps be used to synthesize mixed-linker of other SOD ZIFs particularly for separation applications.

Supplementary Information The online version contains supplementary material available at https://doi.org/10.1007/s11814-024-00192-4.

Acknowledgements The authors would like to acknowledge financial supports by the Ministry of Higher Education of Malaysia under the Fundamental Research Grant Scheme (FRGS/1/2021/TK0/UPM/02/10)—Investigation of Crystal Nucleation, Diffusion, and Sorption Properties of Isostructural Dual-Linker SOD Zeolitic-Imidazolate Framework Crystals

Declarations

Conflict of Interest The authors declare that they have no known competing financial interests or personal relationships that could have appeared to influence the work reported in this paper.

References

1. Q. Qian et al., Chem. Rev. **120**, 8161–8266 (2020)
2. L.M. Robeson, J. Membr. Sci. **320**, 390–400 (2008)
3. A.R. Kamble, C.M. Patel, Z.V.P. Murthy, Renew. Sustain. Energy Rev. **145**, 111062 (2021)
4. M.R.A. Hamid, H.-K. Jeong, Korean J. Chem. Eng. **35**, 1577–1600 (2018)
5. K.S. Park, Z. Ni, A.P. Côté, J.Y. Choi, R. Huang, F.J. Uribe-Romo, H.K. Chae, M. O'Keeffe, O.M. Yaghi, Proc. Natl. Acad. Sci. U.S.A. **103**, 10186–10191 (2006)
6. R. Banerjee, A. Phan, B. Wang, C. Knobler, H. Furukawa, M. O'Keeffe, O.M. Yaghi, Science **319**, 939–943 (2008)

7. M.R. Abdul Hamid, T.C. Shean Yaw, M.Z. Mohd Tohir, W.A. Wan Abdul Karim Ghani, P.D. Sutrisna, H.-K. Jeong, J. Ind. Eng. Chem. **98**, 17–41 (2021)
8. C. Zhang, R.P. Lively, K. Zhang, J.R. Johnson, O. Karvan, W.J. Koros, J. Phys. Chem. Lett. **3**, 2130–2134 (2012)
9. P. Krokidas, S. Moncho, E.N. Brothers, M. Castier, I.G. Economou, Phys. Chem. Chem. Phys. **20**, 4879–4892 (2018)
10. J.A. Thompson, C.R. Blad, N.A. Brunelli, M.E. Lydon, R.P. Lively, C.W. Jones, S. Nair, Chem. Mater. **24**, 1930–1936 (2012)
11. A. Dhakshinamoorthy, A.M. Asiri, H. Garcia, Catal. Sci. Technol. **6**, 5238–5261 (2016)
12. F. Hillman, J.M. Zimmerman, S.-M. Paek, M.R.A. Hamid, W.T. Lim, H.-K. Jeong, J. Mater. Chem. A **5**, 6090–6099 (2017)
13. C. Wang, F. Yang, L. Sheng, J. Yu, K. Yao, L. Zhang, Y. Pan, Chem. Commun. **52**, 12578–12581 (2016)
14. J. Sun, L. Semenchenko, W.T. Lim, M.F. Ballesteros Rivas, V. Varela-Guerrero, H.-K. Jeong, Microporous Mesoporous Mater. **264**, 35–42 (2018)
15. F. Hillman, J. Brito, H.-K. Jeong, ACS Appl. Mater. Interfaces **10**, 5586–5593 (2018)
16. Q. Hou, Y. Wu, S. Zhou, Y. Wei, J. Caro, H. Wang, Angew. Chem. Int. Ed. **58**, 327–331 (2019)
17. K. Eum et al., J. Am. Chem. Soc. **137**, 4191–4197 (2015)
18. F. Hillman, H.-K. Jeong, ACS Appl. Mater. Interfaces **11**, 18377–18385 (2019)
19. S. Berens, F. Hillman, M.R. Abdul Hamid, H.-K. Jeong, S. Vasenkov, Microporous Mesoporous Mater. **315**, 110897 (2021)
20. S. Park, H.-K. Jeong, J. Membr. Sci. **596**, 117689 (2020)
21. X.-C. Huang, Y.-Y. Lin, J.-P. Zhang, X.-M. Chen, Angew. Chem. Int. Ed. **45**, 1557–1559 (2006)
22. F. Hillman, M.R.A. Hamid, P. Krokidas, S. Moncho, E.N. Brothers, I.G. Economou, H.-K. Jeong, Angew. Chem. Int. Ed. **60**, 10103–10111 (2021)
23. S.R. Venna, J.B. Jasinski, M.A. Carreon, J. Am. Chem. Soc. **132**, 18030–18033 (2010)
24. Q. Bao, Y. Lou, T. Xing, J. Chen, Inorg. Chem. Commun. **37**, 170–173 (2013)
25. M.R. Abdul Hamid, H.-K. Jeong, J. Ind. Eng. Chem. **88**, 319–327 (2020)
26. M. Arivazhagan, S. Manivel, S. Jeyavijayan, R. Meenakshi, Spectrochim. Acta A Mol. Biomol. Spectrosc. **134**, 493–501 (2015)
27. D. Fairen-Jimenez, S.A. Moggach, M.T. Wharmby, P.A. Wright, S. Parsons, T. Düren, J. Am. Chem. Soc. **133**, 8900–8902 (2011)
28. J. Ahn, W.-J. Chung, I. Pinnau, M.D. Guiver, J. Membr. Sci. **314**, 123–133 (2008)
29. R.J. Verploegh, Y. Wu, D.S. Sholl, Langmuir **33**, 6481–6491 (2017)
30. X. Mei, S. Yang, P. Lu, Y. Zhang, J. Zhang, Front. Chem. **8**, 1–10 (2020)
31. N.A.H. Md. Nordin, A.F. Ismail, A. Mustafa, R.S. Murali, T. Matsuura, RSC Adv. **5**, 30206–30215 (2015)
32. M.J.C. Ordoñez, K.J. Balkus, J.P. Ferraris, I.H. Musselman, J. Membr. Sci. **361**, 28–37 (2010)